Supporting Information

Metal-organic framework with pore contraction and modification by diethylammonium cations for record SO_2/CO_2 separation

Mei Yang,[a,#] Wenke Yuan,[a,#] Xiu-Yuan Li,[b,] Bo Liu[a] and Huifang Zhou[a,*]*

[a] College of Chemistry & Pharmacy, Northwest A&F University, Yangling 712100, P. R. China.

[b] School of Materials Science and Chemical Engineering, Xi'an Technological University, Xi'an 710032, China.

To whom correspondence should be addressed.

E-mail: lixiuyuan@xatu.edu.cn (Xiu-Yuan Li)

E-mail: hfzhou@nwafu.edu.cn (Huifang Zhou)

Experimental Section

Materials and general characterizations

The study utilized analytical-grade reagents, which were commercially available. Powder X-ray diffraction (PXRD) analysis was conducted using a Bruker D8 ADVANCE powder X-ray diffractometer equipped with Cu Kα radiation (λ = 1.5406 Å). Thermogravimetric analysis (TGA) was performed under a nitrogen atmosphere at a constant heating rate of 10 °C per minute, employing a NETZSCH TG 209 F3 instrument. Fourier transform infrared (FT-IR) spectroscopy measurements were performed on a Nicolet Avatar 360 FT-IR instrument. Elemental analysis was performed in an Elementar UNICUBE.

Synthesis of Zn-DPNA

The synthesis of **Zn-DPNA** was achieved by combining $Zn(NO_3)_2 \cdot 6H_2O$ (17.9 mg) and 5-(2′,5′-dicarboxylphenyl)nicotinic acid (H_3DPNA, 7.3 mg) in a 10 mL screw-cap glass vial. The mixture was then supplemented with *N*,*N*-diethylformamide (DEF, 2.0 mL) and a dilute solution of nitric acid (HNO_3:H_2O = 1:10, 0.5 mL). Subsequently, the mixture underwent ultrasonication to ensure thorough mixing and homogeneity. Following ultrasonication, the vial was sealed and heated at 120 °C for 48 hours to facilitate the formation of the samples. Upon completion of the heating process, the reaction mixture was allowed to cool to room temperature, the resulting colorless rod-shaped crystals were harvested via filtration. The crystals were washed with DEF to remove any unreacted precursors. The as-synthesized samples then exchanged with dichloromethane for 3 days, followed by activation at 100 °C under vacuum for 8 h. $(Et_2NH_2)[Zn_{5.5}(DPNA)_4]$ elemental analysis Calcd. (%): C = 45.88, H = 2.31, N = 4.46; Found (%): C = 44.92, H = 3.06, N = 4.22. FT-IR (4000-400 cm^{-1}, see Fig. S10): 3433 (br), 1610 (s), 1369 (s), 1268 (w), 1137 (m), 1049 (m), 917 (w), 832 (m), 780 (m), 707 (m), 580 (s).

X-ray Crystallography

The X-ray diffraction data were collected using a Bruker APEX-II CCD area detector diffractometer with Cu Kα radiation (λ = 1.54178 Å). The structure was solved by direct method and refined by a full-matrix least-squares method. All non-hydrogen atoms were

refined with anisotropic displacement parameters. Solvent masks are applied after all the atoms are located. The crystallographic data for the MOF are presented in Table S1. This table includes details such as cell dimensions, space group, and structural refinement parameters, providing a comprehensive overview of the crystal structure's precision and quality.

Adsorption/desorption experiments

The synthesized sample of **Zn-DPNA** is placed in dichloromethane and allowed to soak for 48 hours. During this process, fresh dichloromethane is replaced every 12 hours to ensure continuous effective cleaning. The soaked sample is then placed in a vacuum environment and dried at 140°C for 8 hours. N_2 adsorption at 77 K was measured on a micromeritics ASAP 2020 Plus adsorption analyzer. The single-component adsorption isotherms of CO_2 at 273 and 298 K were measured using a micromeritics ASAP 2020 Plus adsorption analyzer. The SO_2 adsorption isotherms at 273 and 298 K were collected using a BSD-PMC corrosive gas adsorption analyzer (Beishide Instrument Technology (Beijing) Co., Ltd.). Cycling adsorption-desorption experiments for SO_2 were conducted on a BSD-PMC corrosive gas adsorption analyzer. Between each cycle, the sample was reactivated at 373 K for 20 minutes.

Grand Canonical Monte Carlo (GCMC) simulations

Grand Canonical Monte Carlo (GCMC) simulations were performed using Materials Studio package. The 2×2×2 supercell was used for the simulations. The partial charges for atoms of the framework were derived from QEq method. All the parameters for atoms of **Zn-DPNA** phases were modeled with the Dreiding forcefield. The LJ potential parameters for SO_2 and CO_2 were taken from the Optimized Potentials for Liquid Simulations–All Atom (OPLS-AA) and TraPPE force field, respectively. A cutoff distance of 7.5 Å was used for LJ interactions, and the Coulombic interactions were calculated by using Ewald summation. For each run, the 5×10^6 equilibration steps, 5×10^6 production steps were employed.

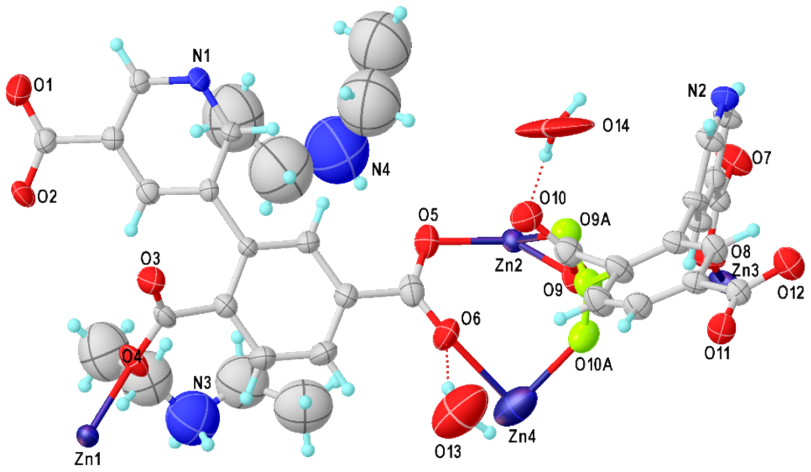

Fig. S1 Asymmetry unit structure of **Zn-DPNA** with thermal ellipsoids set at 50% probability level. The second disordered component of carboxyl was colored as green.

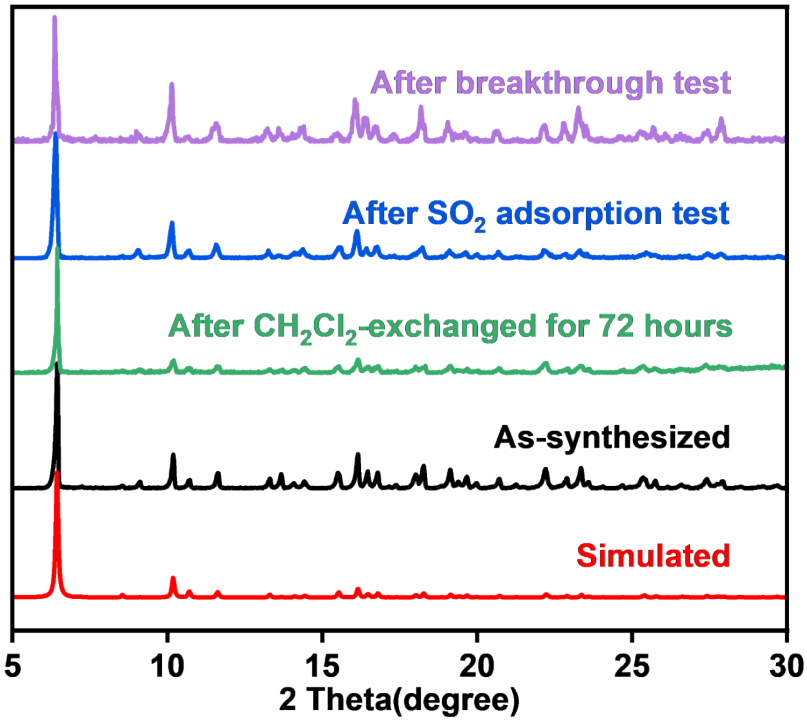

Fig. S2 PXRD of the single crystal simulated, as-synthesized, CH_2Cl_2-exchanged **Zn-DPNA**, and **Zn-DPNA** after adsorption and breakthrough tests.

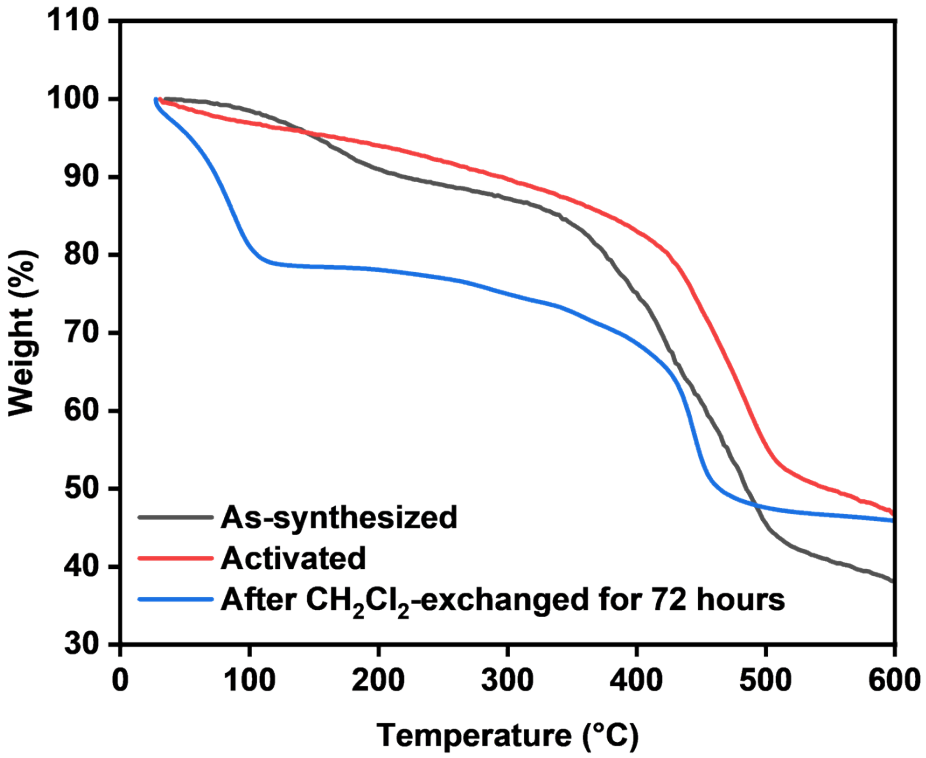

Fig. S3 TGA curves of the as-synthesized, activated and CH_2Cl_2-exchanged **Zn-DPNA** under N_2 atmosphere. The TGA cure of the activated sample shows a slight weight loss before 350 ^oC indicates possible guest water molecules removal from the structure. This slight weight reduction may be attributed to the re-adsorption of water vapor from the ambient air by the activated sample prior to testing.

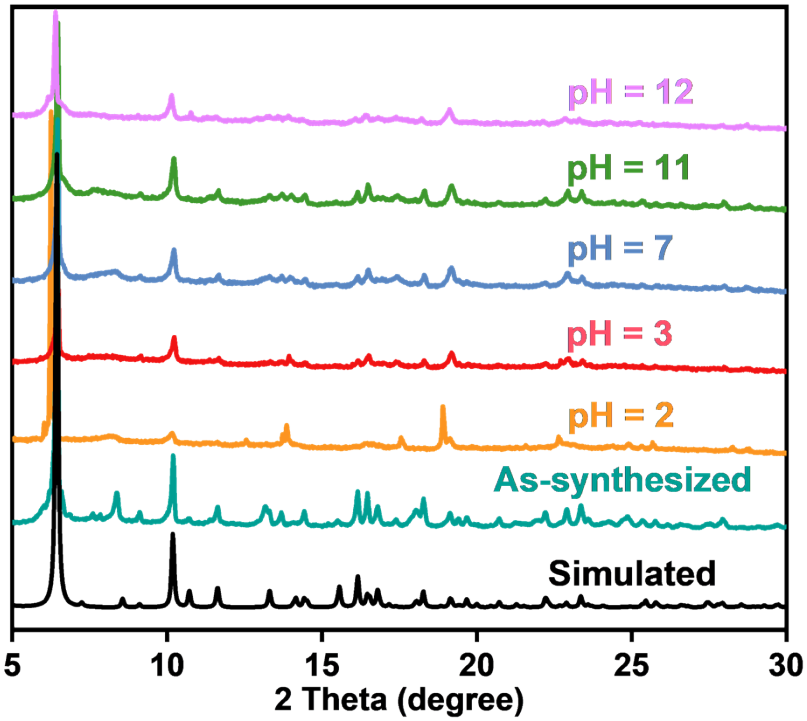

Fig. S4 PXRD of single crystal simulated, as-synthesized **Zn-DPNA** and **Zn-DPNA** after being soaked in the solution of different pH.

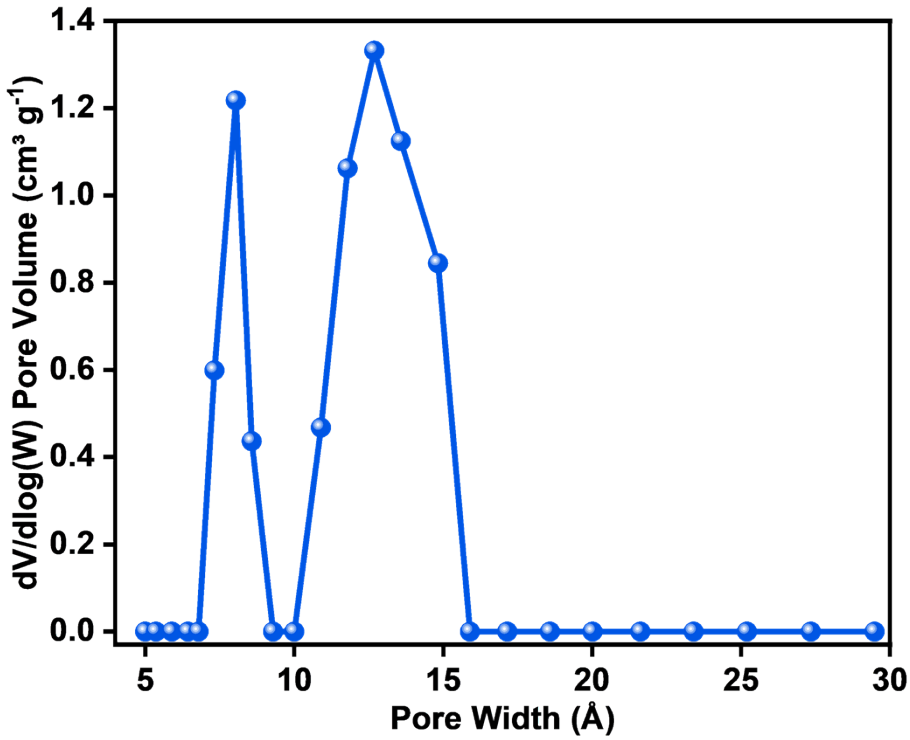

Fig. S5 Pore size distribution of **Zn-DPNA** calculated by the Non-Local Density Functional Theory (NLDFT).

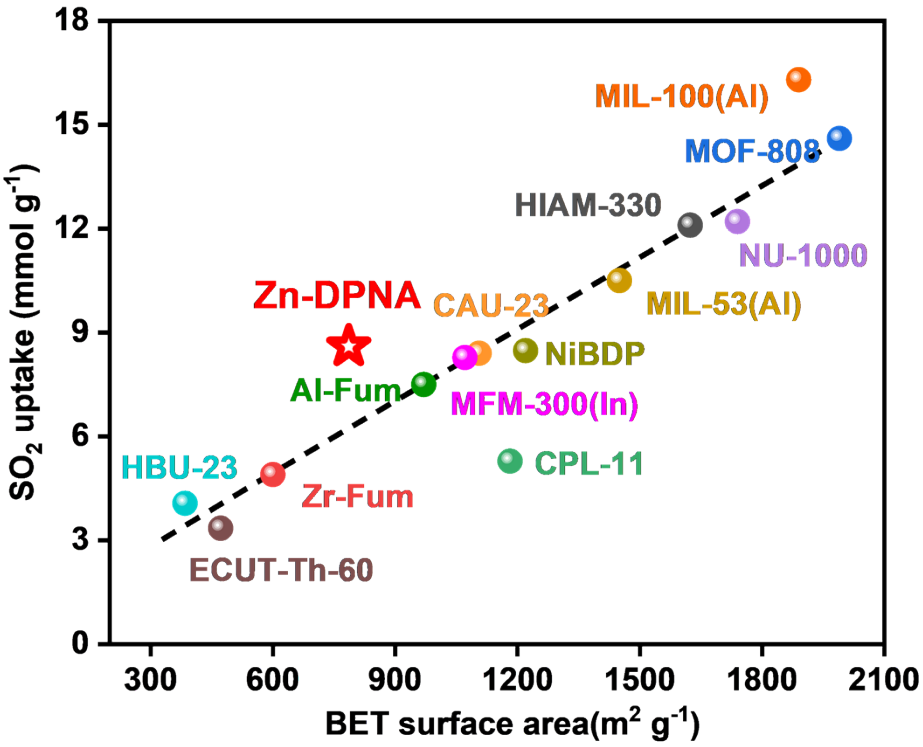

Fig. S6 Plot of the SO_2 adsorption capacity and BET surface area for **Zn-DPNA** and other top-performing MOFs.

Calculation of sorption heat for gas uptakes using Virial II model

$$\ln P = \ln N + 1/T\Sigma_{i=0}^{m} a_i N^i + \Sigma_{i=0}^{n} b_i N^i \quad \text{(eq. S1)}$$

$$Q_{st} = -R\sum_{i=0}^{m} a_i N^i \quad \text{(eq. S2)}$$

The eq. S1 was applied to fit the combined gas isotherm data for **Zn-DPNA** at 273 K and 298 K, where P is the pressure, N is the adsorbed amount, T is the temperature, a_i and b_i are virial coefficients, and m and n are the number of coefficients used to describe the isotherms. Q_{st} in eq. S2 is the coverage-dependent enthalpy of adsorption and R is the universal gas constant. The fitting results are given in Table S3.

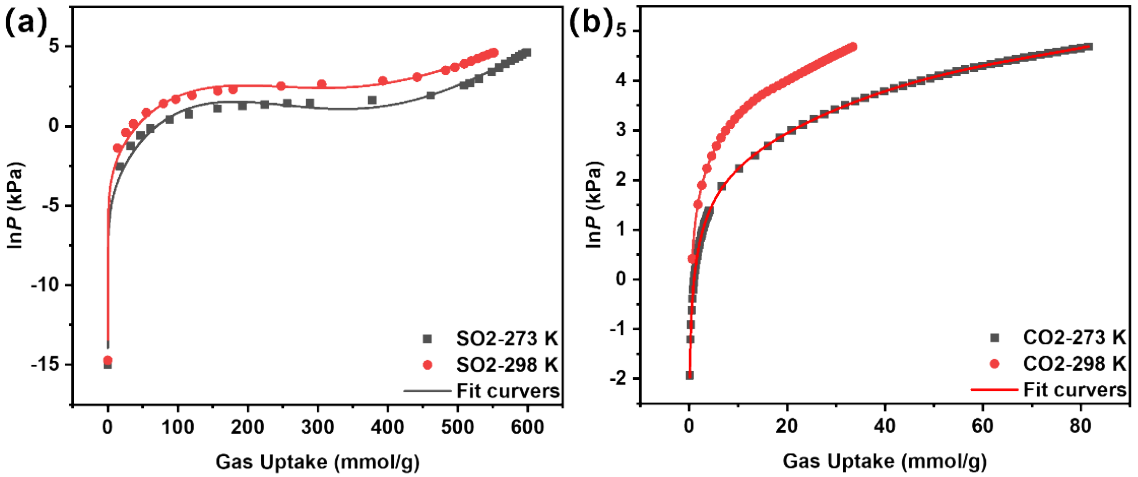

Fig. S7 The virial fitting of the SO_2 (a) and CO_2 (b) adsorption isotherms for **Zn-DPNA** at 273 and 298 K.

Calculation of IAST selectivity

Single-component gas equilibrium adsorption isotherms were fitted with dual-site Langmuir–Freundlich (DSLF) model, given by the following equation:

$$N = A_1 \frac{b_1 p^{c_1}}{1 + b_1 p^{c_1}} + A_2 \frac{b_2 p^{c_2}}{1 + b_2 p^{c_2}} \quad \text{(eq. S3)}$$

where N is the amount of adsorbed gas (mmol·g $^{-1}$), p is the bulk gas phase pressure (atm), A_1 and A_2 are the adsorption saturation capacity for site 1 and site 2 (mmol·g $^{-1}$), b_1 and b_2 are the affinity coefficients of site (1/kPa), c_1 and c_2 are the Langmuir–Freundlich exponent (dimensionless) for two adsorption sites A and B indicating the presence of weak and strong adsorption sites.

The parameters of A_1, A_2, b_1, b_2, and c_1, c_2 were then used to predict the adsorption selectivity based on IAST, which is finally defined as:

$$S_{\frac{1}{2}} = \left(\frac{x_1}{x_2}\right)\left(\frac{y_2}{y_1}\right) \quad \text{(eq. S4)}$$

In eq.S4, S is the ideal selectivity of component 1 over component 2, where x_i and y_i are the mole fractions of component i (i = 1 and 2) in the adsorbed and bulk phases, respectively.

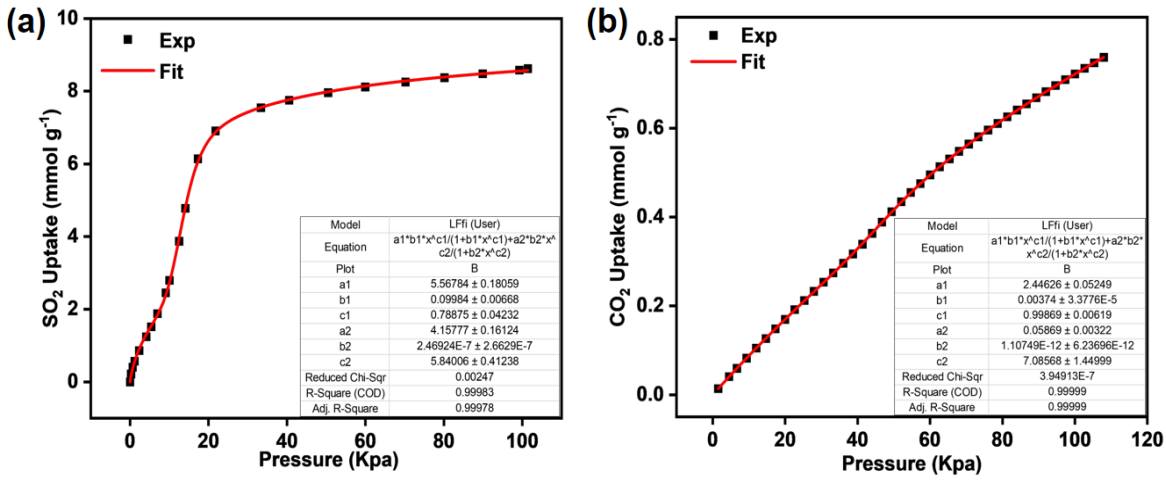

Fig. S8 DSLF fit of the SO_2 and CO_2 adsorption isotherm of **Zn-DPNA** at 298 K with dual-site Langmuir-Freundlich model fits.

Breakthrough experiments

The breakthrough experiment was performed on the BSD-MAB Multicomponent Adsorption Breakthrough Curve Analyzer at 298 K and 1 bar. A stainless-steel column with a length of 70 mm and an inner diameter of 6 mm was used for sample packing. Activated crystalline sample (1~1.2 g) was packed into the column. The column is placed in a circulating jacket connected to the thermostatic bath to control the temperature. Pressure control valve and mass flow controller are used to control the flow and pressure of the gas mixture. Outlet effluent from the column was continuously monitored using gas analytical mass spectrometer. The column packed with sample was firstly activated with N_2 flow of 10 mL min^{-1} for 8 h at 433 K. Between two breakthrough experiments, the adsorbent was regenerated by N_2 flow of 10 mL min^{-1} for 20 min at 373 K to guarantee complete removal of the adsorbed gases.

On the basis of the mass balance, the gas adsorption capacities can be determined as follows:

$$Q_i = \frac{C_i V}{22.4 \times m} \times \int_0^t (1 - \frac{F}{F_0}) dt$$

Where Q_i is the equilibrium adsorption capacity of gas i (mmol g^{-1}), C_i is the feed gas concentration, V is the volumetric feed flow rate (mL min^{-1}), t is the adsorption time (min), F_0 and F are the inlet and outlet gas molar flow rates, respectively, and m is the mass of the adsorbent (g).

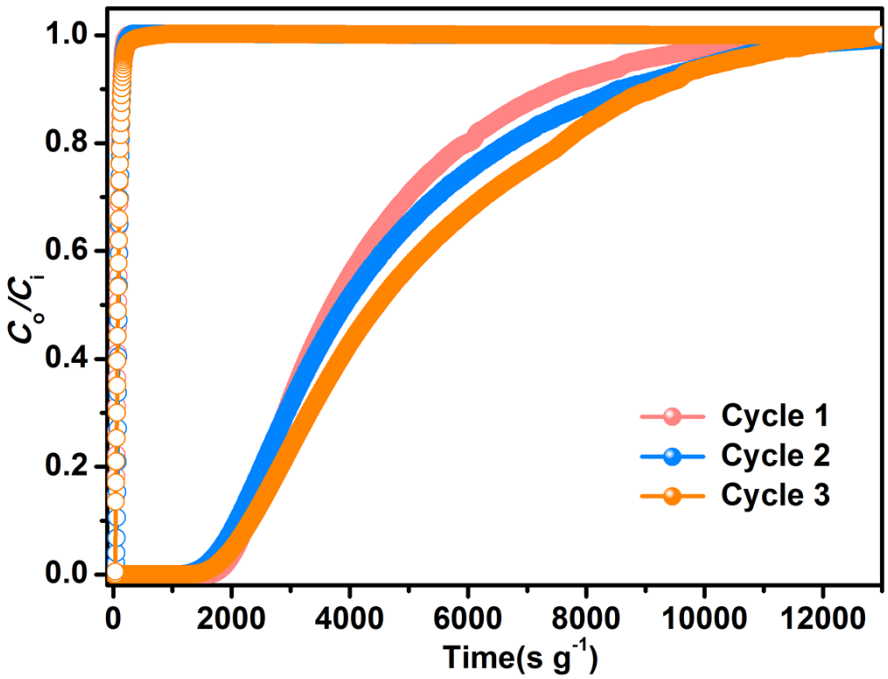

Fig. S9 Three cycling breakthrough experiments for SO_2/CO_2 mixture (2500 ppm SO_2, 15% CO_2 in He) with a total flow rate of 20 mL min^{-1} at 298 K.

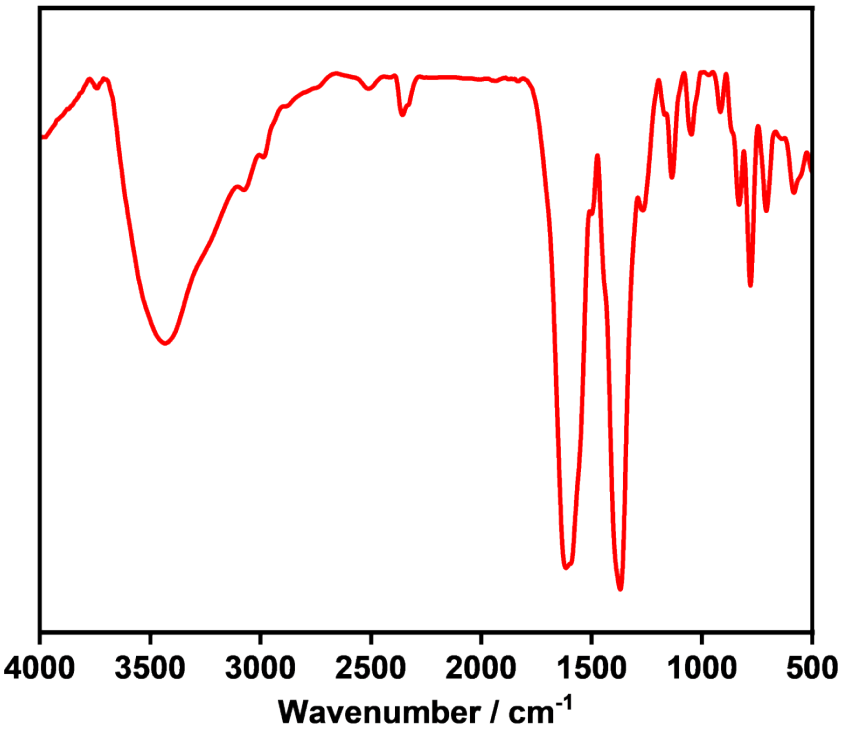

Fig. S10 Fourier-transform infrared (FT-IR) spectra of **Zn-DPNA**.

Table S1. The crystallography data of **Zn-DPNA**.

Identification code	**Zn-DPNA**.
Empirical formula	$C_{60}H_{38}N_5O_{25}Zn_{5.5}$
Formula weight	1588.49
Temperature/K	220.00(10)
Crystal system	tetragonal
Space group	$I\text{-}4_2d$
a/Å	38.8022(8)
b/Å	38.8022(8)
c/Å	12.8725(4)
α/°	90
β/°	90
γ/°	90
Volume/Å^3	19381.0(10)
Z	8
ρ_{calc}g/cm^3	1.089
μ/mm^{-1}	2.001
F(000)	6384
Crystal size/mm^3	0.28 × 0.13 × 0.12
Radiation	CuKα (λ = 1.54178)
2θ range for data collection/°	6.442 to 149.484
Reflections collected	79762
Independent reflections	9688 [R_{int} = 0.1074, R_{sigma} = 0.0542]
Data/restraints/parameters	9688/200/537
Goodness-of-fit on F^2	1.021
Final R indexes [I>=2σ (I)]	R_1 = 0.0517, wR_2 = 0.1385
Final R indexes [all data]	R_1 = 0.0641, wR_2 = 0.1482
Flack parameter	0.46(4)

Table S2. Comparation of the SO_2 uptake, BET surface area and selectivity of the SO_2/CO_2 (50/50 and 10/90, v/v) breakthrough for some reported MOFs.

Material	SO_2 uptake (mmol g^{-1})	BET surface area (m^2 g^{-1})	Selectivity of SO_2/CO_2 (50/50, v/v)	Selectivity of SO_2/CO_2 (10/90, v/v)	Reference
Zn-DPNA	8.6	786	1182	82	This work
Zr-Fum	4.9	600	41	46	1
MOF-808	14.6	1990	370	66	
DUT-67(Zr)	9	1260	37	22	
NU-1000	12.2	1740	22	17	
MIL-53(Al)	10.5	1450	43	22	
NH_2-MIL-53(Al)	8	620	56	42	
Al-Fum	7.5	970	36	35	
MIL-53(tdc)(Al)	6.9	1000	83	48	
MIL-96(Al)	6.5	530	8	7	
MIL-100(Al)	16.3	1890	38	18	
NH_2-MIL-101(Al)	17.3	1770	16	20	
CAU-23	8.4	1106	48	34	2
HIAM-330	12.1	1624	60	44	3
MFM-300(In)	8.28	1071	47	-	4
HBU-20	6.69	1551.1	-	44.3	5
CPL-11	5.29	1182	-	132	6
Zr-TPA-FA	22.7	2150	-	20.6	7
Zr-TPA-HAc	19.6	1740	-	-	
HBU-23	4.07	384.2	-	58.9	8
DMOF-TM	9.68(293K)	-	253	169	9
ECUT-Th-60	3.35	472	-	-	10
NiBDP	8.48	1220	-	-	11

Table S3. Fitting results of SO_2 and CO_2 adsorption isotherms of **Zn-DPNA**.

Parameter	SO_2	CO_2
b_0	12.62727	10.68538
b_1	-0.06823	0.38343
b_2	3.14937E-4	-0.02192
b_3	-3.65693E-7	3.91825E-4
a_0	-5329.34531	-2915.48342
a_1	34.21113	-108.9498
a_2	-0.17251	6.22469
a_3	2.70066E-4	-0.11066
a_4	-1.04811E-7	1.87879E-5
Chi^2	0.14819	1.1852E-4
R^2	0.99183	0.99996

Reference

(1) P. Brandt, S.-H. Xing, J. Liang, G. Kurt, A. Nuhnen, O. Weingart and C. Janiak, *ACS Appl. Mater. Interfaces,* 2021, **13**, 29137-29149.

(2) C. Jansen, N. Tannert, D. Lenzen, M. Bengsch, S. Millan, A. Goldman, D. N. Jordan, L. Sondermann, N. Stock and C. Janiak, *Z. Anorg. Allg. Chem.,* 2022, **648**, e202200170.

(3) L. Yu, M. He, J. Yao, Q. Xia, S. Yang, J. Li and H. Wang, *Chem. Sci.,* 2024, **15**, 8530-8535.

(4) M. Savage, Y. Cheng, T. L. Easun, J. E. Eyley, S. P. Argent, M. R. Warren, W. Lewis, C. Murray, C. C. Tang, M. D. Frogley, G. Cinque, J. Sun, S. Rudić, R. T. Murden, M. J. Benham, A. N. Fitch, A. J. Blake, A. J. Ramirez-Cuesta, S. Yang and M. Schröder, *Adv. Mater.,* 2016, **28**, 8705-8711.

(5) Y.-B. Ren, H.-Y. Xu, S.-Q. Gang, Y.-J. Gao, X. Jing and J.-L. Du, *Chem. Eng. J.,* 2022, **431**, 134057.

(6) L.-Z. Yang, W. Xie, L. Yan, Q. Fu, X. Yuan, Q. Zheng and X. Zhao, *Sep. Purif. Technol.,* 2024, **346**, 127513.

(7) W. Gong, Y. Xie, A. Yamano, S. Ito, X. Tang, E. W. Reinheimer, C. D. Malliakas, J. Dong, Y. Cui and O. K. Farha, *J. Am. Chem. Soc.,* 2023, **145**, 26890-26899.

(8) S.-Q. Gang, Z.-Y. Liu, Y.-N. Bian, R. Wang and J.-L. Du, *Sep. Purif. Technol.,* 2024, **335**, 126153.

(9) S. Xing, J. Liang, P. Brandt, F. Schäfer, A. Nuhnen, T. Heinen, I. Boldog, J. Möllmer, M. Lange, O. Weingart and C. Janiak, *Angew. Chem. Int. Ed.,* 2021, **60**, 17998-18005.

(10) W. Zhang, W. Jia, J. Qin, L. Chen, Y. Ran, R. Krishna, L. Wang and F. Luo, *Inorg. Chem.,* 2022, **61**, 11879-11885.

(11) J. L. Obeso, K. Gopalsamy, M. Wahiduzzaman, E. Martínez-Ahumada, D. Fan, H. A. Lara-García, F. J. Carmona, G. Maurin, I. A. Ibarra and J. A. R. Navarro, *J. Mater. Chem. A,* 2024, **12**, 10157-10165.